Oxo- and Hydroxo-Bridged Heme-Copper Assemblies Formed from Acid−Base or Metal−Dioxygen Chemistry

Marie-Aude Kopf,† Yorck-Michael Neuhold,‡ Andreas D. Zuberbühler,‡ and Kenneth D. Karlin*,†

Department of Chemistry, The Johns Hopkins University, Baltimore, Maryland 21218, and Institut für Anorganische Chemie, University of Basel, CH-4056 Basel, Switzerland

Received December 15, 1998

The iron−copper dinuclear active site in heme-copper oxidases (e.g., cyctochrome *c* oxidase) has spurred the development of the inorganic chemistry of bridged heme-copper complexes, including species possessing (porphyrinate)Fe^{III}−O(H)−Cu^{II}−L moieties. We describe here the synthesis, by two routes, of [(F_8TPP)Fe^{III}−O−Cu^{II}(MePY2)]$^+$ (**5**) {F_8TPP = tetrakis(2,6-difluorophenyl)porphyrinate; MePY2 = *N*,*N*-bis[2-(2-pyridyl)ethyl]-methylamine}. First, **5-(CF_3SO_3)** was generated by reaction of [(MePY2)Cu^{II}](CF_3SO_3)$_2$ (**3-(CF_3SO_3)$_2$**) and [(F_8TPP)Fe^{III}−OH] (**4**) with triethylamine in THF or CH_3CN in 65−70% yield. The complex was also prepared by reduction of O_2 by a 1:1 mixture of copper(I) and iron(II) complexes, [(MePY2)Cu^I(CH_3CN)](BArF) (**1-(BArF)**) (BArF = tetrakis(3,5-bis-trifluoromethylphenyl)borate) and (F_8TPP)Fe^{II} (**2**) in O_2-saturated THF or acetone, at −80 °C with subsequent warming to room temperature. Preliminary stopped-flow kinetics on the O_2 reaction with the 1:1 mixture show the formation of at least two intermediates (i.e., a superoxo species (F_8TPP)Fe−O_2 first, and then a presumed peroxo-bridged Fe−O_2−Cu species) prior to the formation of the final *μ*-oxo complex [(F_8TPP)Fe^{III}−O−Cu^{II}(MePY2)]$^+$ (**5-(BArF)**). The ^{1}H NMR spectrum of **5-(CF_3SO_3)** in CD_2Cl_2 exhibits a pyrrole peak at 67.7 ppm (corroborated by ^{2}H NMR), while downfield (23.4 and 18.9 ppm) and dramatically upfield-shifted resonances (−87.7, −155.4 and −189.4) have been assigned to hydrogens of the MePY2 moiety, by specific deuteration. The *μ*-hydroxo complex [(F_8TPP)Fe−(OH)−Cu(MePY2)](OTf)$_2$ (**6-(CF_3SO_3)$_2$**) was synthesized by addition of **3-(CF_3SO_3)$_2$** to **4** in CH_3CN, or by protonation of **5-(CF_3SO_3)** with CF_3SO_3H. In a ^{1}H NMR-spectroscopic protonation titration (CF_3SO_3H), the pyrrole 67.7 ppm resonance for **5-(CF_3SO_3)** progressively converts to 70.3 ppm, diagnostic of **6-(CF_3SO_3)$_2$**. The protonation is slow on the NMR time scale. The ^{1}H NMR spectral properties are consistent with antiferromagnetically coupled high-spin iron(III) and Cu(II) ions ($S = 2$ spin state), and the interaction is weaker in **6-(CF_3SO_3)$_2$** (**5-(CF_3SO_3)**, $\mu_{eff} = 5.05\ \mu_B$; **6-(CF_3SO_3)$_2$**, $\mu_{eff} = 5.60\ \mu_B$; Evans NMR method). By titration using a series of organic acids, the pK_a for **6-(CF_3SO_3)$_2$** has been estimated to be 16.7 < pK_a < 17.6 (CH_3CN solvent), or 9.6 ± 2 (aqueous). Plots of δ vs 1/T for both *μ*-oxo and *μ*-hydroxo complexes **5-(CF_3SO_3)** and **6-(CF_3SO_3)$_2$** have been obtained, showing linear Curie (for downfield resonances) or anti-Curie (for upfield peaks) behavior.

Introduction

The characterization of (P)Fe^{III}−X−Cu^{II}(ligand) species (X = bridging ligand; P = porphyrinate) has generated considerable interest.[1,2] Elucidating synthetic strategies and determining physical and chemical properties of such bridged heme-copper assemblies is in large part inspired by our current knowledge of the active site structure and chemistry of heme-copper oxidases such as cytochrome *c* oxidase.[3] Here, the active site where O_2 binding and reduction occurs consists of a high-spin heme group (with proximal histidine), which lies at ~4.5 Å[4,5] from Cu_B, which possesses three histidine nitrogen ligands. Adjacent or bridged heme-copper centers have thus been targeted for biomimetic modeling studies, with particular recent attention concentrated on compounds with the X being cyano (CN^-),[6−10] carboxylato (RCO_2^-),[11] oxo (O^{2-}), and hydroxo (OH^-)[12−17] bridging ligands.

In particular, *μ*-oxo and *μ*-hydroxo heme-copper complexes have drawn our attention. While proposed[18,19] quite early as a

* Author for correspondence.
† Johns Hopkins University.
‡ University of Basel.

(1) Kopf, M.-A.; Karlin, K. D. In *Biomimetic Oxidations*; Meunier, B., Ed.; Imperial College Press: London, 1999; Chapter 7, in press.
(2) Kitajima, N. *Adv. Inorg. Chem.* **1992**, *39*, 1−77.
(3) (a) Ferguson-Miller, S.; Babcock, G. T. *Chem. Rev.* **1996**, *96*, 2889−2907. (b) Michel, H.; Behr, J.; Harrenga, A.; Kannt, A. *Annu. Rev. Biophys. Biomol. Struct.* **1998**, *27*, 329−356.
(4) Yoshikawa, S.; Shinzawa-Itoh, K.; Nakashima, R.; Yaono, R.; Yamashita, E.; Inoue, N.; Yao, M.; Jei-Fei, M.; Libeu, C. P.; Mizushima, T.; Yamaguchi, H.; Tomizaki, T.; Tsukihara, T. *Science* **1998**, *280*, 1723−1729.
(5) Ostermeier, C.; Harrenga, A.; Ermler, U.; Michel, H. *Proc. Natl. Acad. Sci. U.S.A.* **1997**, *94*, 10547−10553.
(6) Scott, M. J.; Holm, R. H. *J. Am. Chem. Soc.* **1994**, *116*, 11357−11367.
(7) Holm, R. H. *Pure Appl. Chem.* **1995**, *67*, 217−224.
(8) Kauffmann, K. E.; Goddard, C. A.; Zang, Y.; Holm, R. H.; Münck, E. *Inorg. Chem.* **1997**, *36*, 985−993.
(9) Lim, B. S.; Holm, R. H. *Inorg. Chem.* **1998**, *37*, 4898−4908.
(10) Corsi, D. M.; Murthy, N. N.; Young, V. G., Jr.; Karlin, K. D. *Inorg. Chem.* **1999**, *38*, 848−858.
(11) Scott, M. J.; Goddard, C. A.; Holm, R. H. *Inorg. Chem.* **1996**, *35*, 2558−2567.
(12) Karlin, K. D.; Nanthakumar, A.; Fox, S.; Murthy, N. N.; Ravi, N.; Huynh, B. H.; Orosz, R. D.; Day, E. P. *J. Am. Chem. Soc.* **1994**, *116*, 4753−4763.
(13) Fox, S.; Nanthakumar, A.; Wikström, M.; Karlin, K. D.; Blackburn, N. J. *J. Am. Chem. Soc.* **1996**, *118*, 24−34.
(14) Nanthakumar, A.; Fox, S.; Murthy, N. N.; Karlin, K. D. *J. Am. Chem. Soc.* **1997**, *119*, 3898−3906.

10.1021/ic981431+ CCC: $18.00
Published on Web 06/05/1999

possible bridging ligand in the extensively studied oxidized resting state enzyme form, $Fe^{III}-(\mu\text{-}O(H))-Cu^{II}$ complexes have now been generated. Their existence is perhaps somewhat surprising in light of the known thermodynamic stability of μ-oxo dinuclear complexes $P-Fe^{III}-O-Fe^{III}-P$. Yet, $P-Fe^{III}-O-Cu^{II}$(ligand) compounds can be generated by acid−base assembly procedures[13,15−17] and/or by dioxygen reactivity with reduced $P-Fe^{II}/Cu^{I}$(ligand) precursors.[1,12,15b,20] Compounds studied in our own laboratories have focused on oxo and hydroxo complexes with the tripodal tetradentate TMPA (tris(2-pyridylmethyl)amine) copper ligand, in either self-assembled[12−14] or tethered heterobinucleating[15] ligand (L) systems (see diagram). Oxo compounds with linear or bent configurations have

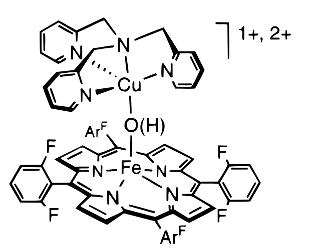

$[(F_8TPP)Fe^{III}\text{-}O(H)\text{-}Cu^{II}(TMPA)]^{+,2+}$

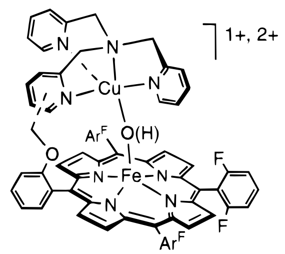

$[(L)Fe^{III}\text{-}O(H)\text{-}Cu^{II}]^{+,2+}$

been characterized. These compounds have novel and interesting magnetic and ^1H NMR properties, and the μ-oxo ligand is very basic, but its protonation behavior depends on the detailed nature of the ligand environment.[15] Such acid−base relationships and proton-transfer chemistry interconverting μ-oxo and μ-hydroxo $Fe^{III}-(\mu\text{-}O(H))-Cu^{II}$ complexes is relevant to enzyme mechanism since heme-copper oxidases function as transmembrane proton pumps. It has been suggested that $Fe^{III}-(\mu\text{-}O(H))-Cu^{II}$ species could represent the resting state enzyme oxidized forms, or possibly could even occur as enzyme turnover intermediates.[13]

In this report, we focus on chemistry with a different copper ligand, *N*,*N*-bis[2-(2-pyridyl)ethyl]methylamine (MePY2). One rationale for previously using TMPA as the copper ligand in heme-copper oxidase model systems was that we have extensively characterized its copper(I)−dioxygen chemistry, preparing us for future studies in $PFe^{II}\cdots Cu^{I}/O_2$ reactivity. We have also described in some detail the dioxygen reactivity of $[(MePY2)Cu^{I}(MeCN)]^+$ (**1**), analogues with N-substituents other then methyl,[21] and binucleating analogues.[22−24]

(15) (a) Obias, H. V.; van Strijdonck, G. P. F.; Lee, D.-H.; Ralle, M.; Blackburn, N. J.; Karlin, K. D. *J. Am. Chem. Soc.* **1998**, *120*, 9696−9697. (b) Ju, T. D.; Ghiladi, R. A.; Lee, D.-H.; van Strijdonck, G. P. F.; Woods, A. S.; Cotter, R. J.; Young, J. V. G.; Karlin, K. D. *Inorg. Chem.* **1999**, *38*, 2244−2245. (c) Kopf, M.-A.; Karlin, K. D., submitted for publication.
(16) Lee, S. C.; Holm, R. H. *J. Am. Chem. Soc.* **1993**, *115*, 5833−5834.
(17) Scott, M. J.; Zhang, H. H.; Lee, S. C.; Hedman, B.; Hodgson, K. O.; Holm, R. H. *J. Am. Chem. Soc.* **1995**, *117*, 568−569.
(18) Blumberg, W. E.; Peisach, J. In *Cytochrome c oxidase*; King, T. e. a., Ed.; Elsevier/North-Holland Biomedical Press: Amsterdam, The Netherlands, 1979; pp 153−159.
(19) Reed, C. A.; Landrum, J. T. *FEBS Lett.* **1979**, *106*, 265−267.
(20) Karlin, K. D.; Lee, D.-H.; Obias, H. V.; Humphreys, K. J. *Pure Appl. Chem.* **1998**, *70*, 855−862.
(21) Sanyal, I.; Mahroof-Tahir, M.; Nasir, S.; Ghosh, P.; Cohen, B. I.; Gultneh, Y.; Cruse, R.; Farooq, A.; Karlin, K. D.; Liu, S.; Zubieta, J. *Inorg. Chem.* **1992**, *31*, 4322−4332.
(22) Karlin, K. D.; Tyeklár, Z.; Farooq, A.; Haka, M. S.; Ghosh, P.; Cruse, R. W.; Gultneh, Y.; Hayes, J. C.; Toscano, P. J.; Zubieta, J. *Inorg. Chem.* **1992**, *31*, 1436−1451.
(23) Obias, H. V.; Lin, Y.; Murthy, N. N.; Pidcock, E.; Solomon, E. I.; Ralle, M.; Blackburn, N. J.; Neuhold, Y.-M.; Zuberbühler, A. D.; Karlin, K. D. *J. Am. Chem. Soc.* **1998**, *120*, 12960−12961.
(24) Pidcock, E.; Obias, H. V.; Abe, M.; Liang, H.-C.; Karlin, K. D.; Solomon, E. I. *J. Am. Chem. Soc.* **1999**, *121*, 1299−1308.

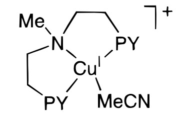

$[(MePY2)Cu^{I}(MeCN)]^+$ (**1**)

These copper(I) complexes with tridentate ligands react with O_2 to give completely different dioxygen adducts, compared to TMPA or its analogues. The tridentate ligands give binuclear μ-η^2:η^2-peroxo−dicopper(II) and/or bis-μ-oxo−dicopper(III) products,[23] while TMPA and its analogues form end-on bound $Cu^{II}-O-O-Cu^{II}$ species.[25] Furthermore, the Cu_B at the Fe−Cu active site of heme-copper oxidases has N_3 (from histidine imidazoles) tridentate coordination.[4,5] Thus, MePY2−copper is worthy of study in association with heme chemistry,[15c] to compare and contrast with TMPA or other systems, with respect to $Fe^{II}-Cu^{I}/O_2$ reactivity, and formation and properties of possible $Fe^{III}-(\mu\text{-}O(H))-Cu^{II}$ products. Furthermore, the tridentate nitrogen ligand in MePY2 matches the number and kind of donor atoms observed at the heme-copper oxidase active site, as mentioned above.

Here, we describe new μ-oxo and μ-hydroxo complexes with the MePY2 ligand on copper, and F_8TPP (tetrakis(2,6-difluorophenyl)porphyrinate) as the iron ligand. As for the TMPA-containing system, we have been successful in generating the μ-oxo product $[(F_8TPP)Fe^{III}-O-Cu^{II}(MePY2)]^+$ (**5**), either by O_2 reactivity with $[(MePY2)Cu^{I}(MeCN)]^+$ (**1**) and $(F_8TPP)Fe^{II}$ (**2**) or by acid−base self-assembly procedures. The synthetic details are presented, and some insights into the oxygenation reaction are provided by low-temperature UV−vis studies, including a preliminary stopped-flow kinetic investigation. The conjugate acid, μ-hydroxo complex $[(F_8TPP)Fe^{III}-OH-Cu^{II}(MePY2)]^{2+}$ (**6**), can be obtained by protonation of **5**, and an estimate of the pK_a of **6** has been determined. In addition to the acid−base interconversion chemistry, the ^1H NMR and magnetic data of **5** and **6** are described.

Results and Discussion

Synthesis of $[(F_8TPP)Fe^{III}-O-Cu^{II}(MePY2)](CF_3SO_3)$ (5-(CF_3SO_3)). Initially, the μ-oxo complex was synthesized by an acid−base self-assembly method, as a triflate salt. Thus, when $[(MePY2)Cu^{II}](CF_3SO_3)_2$ (**3-(CF_3SO_3)$_2$**) is reacted with an equimolar quantity of the iron−hydroxo complex $[(F_8TPP)Fe^{III}-OH]$ (**4**) in the presence of Et_3N, a microcrystalline black precipitate **5-(CF_3SO_3)** can be isolated in high yield (Scheme 1). This preparation is directly analogous to that carried out for the TMPA analogue $[(F_8TPP)Fe^{III}-O-Cu^{II}(TMPA)]^+$.[12,13] Compound **5-($CF_3SO_3$)** is very moisture sensitive, but otherwise stable, and is soluble in a variety of solvents including tetrahydrofuran (THF), acetonitrile, dichloromethane, and acetone. The triflate anion is probably uncoordinated, which is consistent with the observed solution conductivity of the complex (molar conductivity, Λ_m (CH_3CN) = 154 Ω cm^2 mol^{-1}, 1:1 electrolyte,[26] Experimental Section) and the fact that **5-(CF_3SO_3)** has properties essentially identical to those of the BArF analogue (BArF = tetrakis(3,5-bis-trifluoromethylphenyl)-borate) $[(F_8TPP)Fe^{III}-O-Cu^{II}(MePY2)](BArF)$ (**5-(BArF)**) (vide infra).

In addition to elemental analysis (Experimental Section), **5-(CF_3SO_3)** possesses characteristics that clearly identify it as

(25) Tyeklár, Z.; Jacobson, R. R.; Wei, N.; Murthy, N. N.; Zubieta, J.; Karlin, K. D. *J. Am. Chem. Soc.* **1993**, *115*, 2677−2689.
(26) Geary, W. J. *Coord. Chem. Rev.* **1971**, *7*, 81−122.

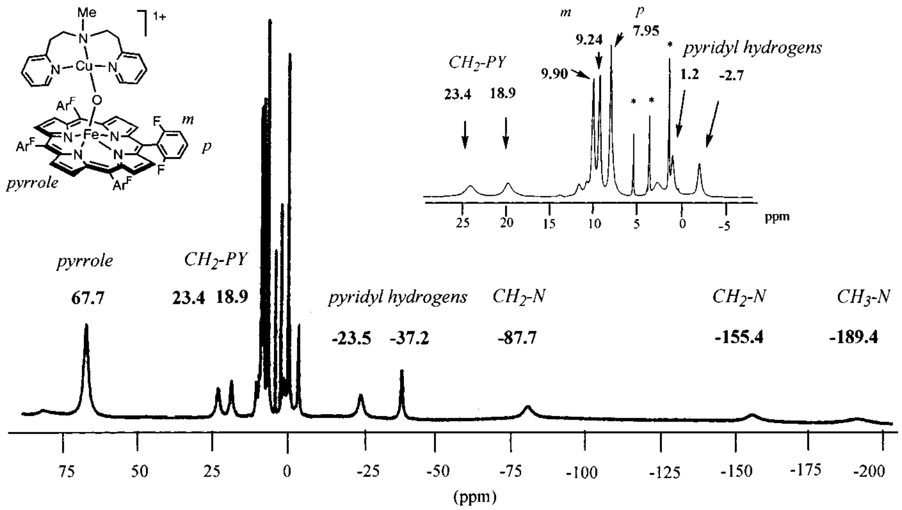

Figure 1. ^{1}H NMR spectrum (297 K) and assignments for **5-(CF$_3$SO$_3$)** in CD_2Cl_2 solvent at 300 MHz. * = solvent peak.

Scheme 1

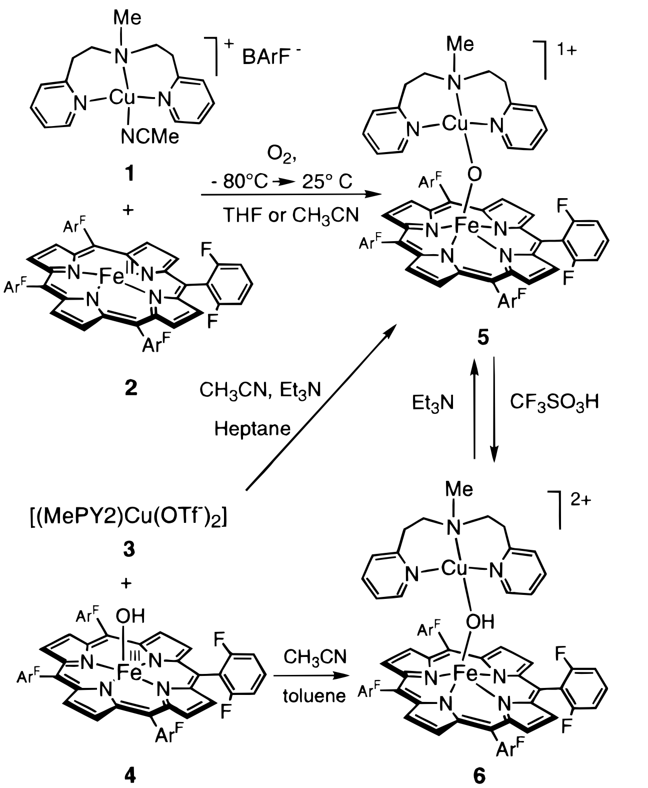

containing the μ-oxo Fe^{III}−O−Cu^{II} moiety. First, **5-(CF$_3$SO$_3$)** has a distinctive red-shifted Soret band (446 nm), which is quite different from high-spin μ-oxo porphyrin−iron(III) dimers such as [(F$_8$TPP)Fe]$_2$O (λ_{max} 400 nm) and (F$_8$TPP)Fe−OH (λ_{max} 408 nm).[12] It has been shown that, in the case of Zn(TPP)L complexes, an increase in negative charge correlates with a decrease in Soret transition energies.[27] Thus, in μ-oxo Fe^{III}−O−Cu^{II} species, the Cu(II) ion is a poorer π-acceptor and has less positive charge than the Fe(III) in corresponding Fe^{III}−O−Fe^{III} complexes. Second, the ^{1}H NMR properties of **5-(CF$_3$SO$_3$)**, discussed in detail below, reveal that it has upfield paramagnetically shifted copper-ligand resonances and downfield-shifted pyrrole absorptions, as seen in [(F$_8$TPP)Fe^{III}−O−Cu^{II}(TMPA)]$^+$.[12,14] Third, a new infrared peak at 837 cm^{-1} is observed for **5-(CF$_3$SO$_3$)**, which is not seen for the starting copper or iron complexes, **3-(CF$_3$SO$_3$)$_2$** and [(F$_8$TPP)Fe^{III}−OH] (**4**). Tentatively, that IR absorption is assigned to the Fe−O−Cu asymmetric stretch, as previously discussed for [(F$_8$TPP)-Fe^{III}−O−Cu^{II}(TMPA)]$^+$ and TMPA-tethered analogues [(L)-Fe^{III}−O−Cu^{II}]$^+$ [15] (see Introduction).

NMR Spectroscopy of 5-(CF$_3$SO$_3$). The room-temperature ^{1}H NMR spectrum of **5-(CF$_3$SO$_3$)** is shown in Figure 1. The most downfield shifted peak at 67.7 ppm is assigned to the pyrrole resonances of the F$_8$TPP portion of the molecule. This assignment was confirmed by synthesis of [(F$_8$TPP-d_8)Fe^{III}−O−Cu^{II}(MePY2)]$^+$ (**5-*d*$_8$**) (Experimental Section) and examination using ^{2}H NMR spectroscopy (Table 1). This pyrrole chemical shift is consistent with high-spin Fe(III), somewhat upfield from the typical value of ~80 ppm seen for (TPP)Fe^{III}−X.[28] The pyrrole resonance in [(F$_8$TPP)Fe^{III}−O−Cu^{II}(TMPA)]$^+$ is in a similar position (Table 1), and as explained for that system,[14] this shift is a result of the antiferromagnetic coupling between the high-spin Fe(III) ($S = {}^{5}/_{2}$) and Cu(II) ($S = {}^{1}/_{2}$) to give an $S = 2$ spin system. Room-temperature magnetic moment measurements on **5-(CF$_3$SO$_3$)**, both in solution ($\mu_{eff} = 5.05\ \mu_B$; Evans method) and in the solid state ($\mu_{eff} = 5.15\ \mu_B$), are consistent with a similar $S = 2$ assignment for **5-(CF$_3$SO$_3$)**; these values are considerably reduced compared to what would be expected for an uncoupled system.[13] The F$_8$TPP meta (*m*) and para (*p*) phenyl hydrogens appear at their usual place, with two peaks observed for the meta protons (9.90 and 9.24 ppm), while the para hydrogens resonate at 7.95 ppm. The split in the *m*-phenyl protons is indicative of different magnetic environments (on the NMR scale, at room temperature), with one set of hydrogens being "up", on the same side of the μ-oxo and copper moieties, while the others are "down". This asymmetry is also observed with the *o*-fluorine atoms with a ^{19}F NMR spectrum of **5-(CF$_3$SO$_3$)** showing a split signal ($\delta = -95.87$ and -96.70 ppm).

By synthesis (Experimental Section) of MePY2-d_7 and MePY2-d_{11} (see diagram) and by a combination of ^{1}H and ^{2}H NMR spectroscopy, the signals at 23.4, 18.9, −87.7, −155.4, and −189.4 ppm have also been unambiguously assigned, Figure 1 and Table 1. The proton signals of a given methylene group are diastereotopic, thus inequivalent, and all individual hydrogen resonances appear. The remaining four signals (−37.2, −23.5,

(27) Nappa, M.; Valentine, J. S. *J. Am. Chem. Soc.* **1978**, *100*, 5075.

(28) Goff, H. M. In *Iron Porphyrins*; Lever, A. B. P., Gray, H. B., Eds.; Addison-Wesley: Reading, MA, 1983; Part 1, Chapter 4.

Table 1. Comparison of Chemical Shifts (ppm) in ^1H and ^2H NMR Spectra of **5**, **6**, and Relevant Compounds

^1H NMR Spectra

	peak position (ppm)					
5	67.7	9.9 9.24	7.95	23.4 18.9	−87.7 −155.4	−189.4
5 (243 K)	81.9	10.7 9.75	8.09	29.8 23.50	−88.2 −209.1	−232.5
6 (243 K)	81.1	12.3 11.47	7.73	32.8 24.8	−120.6, −168.4, −184	
$[(F_8TPP)Fe^{III}-O-Cu^{II})(TMPA)]^+$ [a]	65	9.6 9.2	7.6		−104	N/A
assignment	pyrrole	*m*-phenyl	*p*-phenyl	CH_2-PY	CH_2-N	CH_3

^2H NMR Spectra

	peak position (ppm)		
$[(d_8\text{-}F_8TPP)Fe^{III}-O-Cu^{II}(MeN)(CH_2CH_2PY)_2]^+$	66.36		
assignment	pyrrole		
$[(F_8TPP)Fe^{III}-O-Cu^{II}(CD_3N)(CH_2CD_2PY)_2]^+$	23.75 19.61	−182.76	
assignment	CD_2-PY	CD_3	
$[(F_8TPP)Fe^{III}-O-Cu^{II})(CD_3N)(CD_2CD_2PY)_2]^+$	24.26 20.20	−75.78 −149	−182.76
assignment	CD_2-PY	CD_2-N	CD_3

[a] Reference 13.

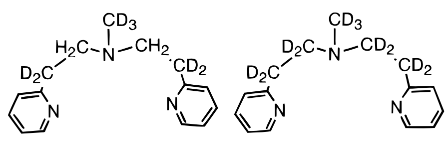

MePY2-d_7 MePY2-d_{11}

−2.7, and 1.2 ppm) must be due to pyridyl ring hydrogen resonances of the MePY2 moiety. Note that the $-C\mathbf{H}_2PY$ methylene hydrogens are downfield shifted, opposite to the direction of the pyridyl ring hydrogens; it is not uncommon for a methylene pair bound to a pyridine ring to have a chemical shift similar in magnitude but opposite in sign to the aromatic proton in the same position.[29,30] A final point is that the pyridyl hydrogen resonance at 1.2 ppm, the least shifted from an expected diamagnetic position, is most likely assigned to the pyridyl 4-hydrogens of the MePY2 copper ligand, since it is the furthest in distance and the highest number of bonds away from the paramagnetic copper ion.

Since monomeric Cu(II) complexes usually do not exhibit well-resolved proton NMR signals, the presence of relatively sharp, upfield-shifted peaks indicates an antiferromagnetic interaction between the iron(III) and copper(II) ions, as mentioned above. The same phenomenon is observed in $[(F_8TPP)Fe^{III}-O-Cu^{II}(TMPA)]^+$, $[(F_8TPP)Fe^{III}-OH-Cu^{II}(TMPA)]^{2+}$ and tethered complexes $[(^5L)Fe^{III}-O-Cu^{II}]^+$,[15] and we have previously presented a detailed discussion of the theoretical framework from Bertini and Luchinat and co-workers,[31] used to interpret these NMR spectra. The upfield *and* downfield peak signature is seen in cobalt(II)-substituted Cu−Zn superoxide dismutase[31,32] and certain forms of iron ferrodoxins.[31] An iron(III) chlorin π-cation radical complex with overall $S = 2$ has also been reported (where the high-spin $S = {}^5/_2$ Fe(III) is antiferromagnetically coupled to a porphyrin $S = {}^1/_2$ radical cation).[33] The behavior of the present $S = 2$ $Fe^{III}-O-Cu^{II}$ complexes with large chemical shift range is unprecedented.

Formation of 5 from Fe/Cu/O$_2$ Reaction. The μ-oxo complex **5-(BArF)** has also been generated directly by reaction of O_2 with the copper(I) and iron(II) complexes. The equimolar mixture of $[(MePY2)Cu^I(CH_3CN)](BArF)$ (**1-(BArF)**) and iron(II) species **2** in THF or acetone, when saturated with dry O_2 at −80 °C, gives, upon warming to room temperature, a red solution of the μ-oxo product (Scheme 1). Its ^1H NMR spectrum is nearly identical to that observed for the acid−base synthetically generated complex, **5-(CF$_3$SO$_3$)** (see Experimental Section).

Some insight into the dioxygen reactivity involved has been obtained from low-temperature UV−vis experiments (Scheme 2 and Figure 2). When **2** ($\lambda_{max} = 422$ nm) is reacted with O_2 at −70 °C in THF, there is an immediate change in the UV−vis spectrum, giving a low-temperature stable species with $\lambda_{max} =$ 416 (Soret) and 536 nm, Figure 2. This has independently been characterized as an Fe/O_2 1:1 adduct, hereafter designated as $(F_8TPP)Fe-O_2$, formally a superoxo−iron(III) complex, with THF acting as an axial ligand.[34] After application of a vacuum to remove excess O_2 {$(F_8TPP)Fe-O_2$ is stable under these conditions}, 1 equiv of **1-(BArF)** was added. The first UV−vis spectrum recorded after ca. 30 s following addition of **1-BArF** and mixing showed that the 416 Soret band shifted to 422 nm (but with much lower intensity than that of pure **2**) while a broad α absorption is observed. (These time-dependent spectral changes are shown in a figure given in the Supporting

(29) Murthy, N. N.; Karlin, K. D.; Bertini, I.; Luchinat, C. *J. Am. Chem. Soc.* **1997**, *119*, 2156−2162.
(30) McConnell, H. M. *J. Chem. Phys.* **1956**, *24*, 632.
(31) Luchinat, C.; Ciurli, S. In *Biological Magnetic Resonance*; Berliner, J., Reuben, J., Eds.; Plenum: New York, 1993; Vol. 12, pp 357−420.
(32) Bertini, I.; Luchinat, C.; Piccioli, M. *Progress in NMR Spectroscopy*; London, 1994.
(33) Ozowa, S.; Watanabe, Y.; Morishima, I. *J. Am. Chem. Soc.* **1994**, *116*, 5832−5838.
(34) Ghiladi, R. A.; Dahan, M.; Neuhold, Y.-M.; Zuberbühler, A. D.; Karlin, K. D. Manuscript in preparation. Characterization of $(F_8TPP)Fe-O_2$ comes from UV−vis and NMR spectroscopic properties (diamagnetic, i.e., with THF axial base ligand), in addition to O_2-uptake ($Fe:O_2 =$ 1:1) measurements.

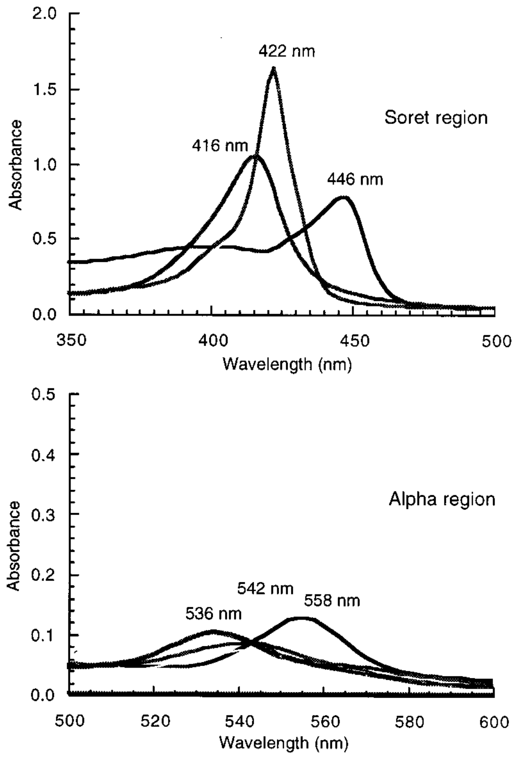

Figure 2. Spectra (Soret and α regions) for O_2 chemistry, leading to formation of the μ-oxo product **5-(BArF)**; 446 (Soret) and 558 nm. Addition of O_2 to **2** (422, 542 nm) gives $(F_8TPP)Fe-O_2$ (416, 536 nm). After removal of excess O_2 and addition of 1 equiv of **1-(BArF)**, **5-(BArF)** is obtained. Also, see Scheme 2 and Supporting Information.

Scheme 2

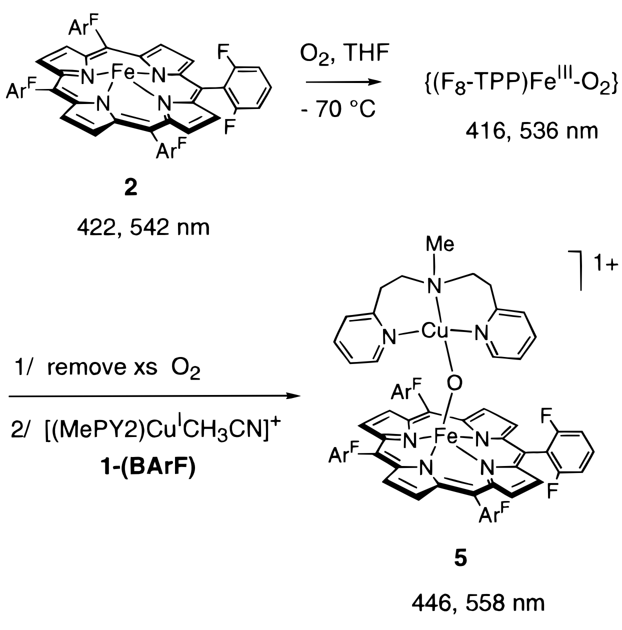

Information). Then, over a period of several hours (still at −70 °C), the complex **5-(BArF)**, with characteristic red-shifted 446 nm Soret and 558 nm α band, forms cleanly.

In acetone, when a 1:1 mixture of **1-(BArF)** and **2** was bubbled with O_2 at −75 °C, a species with very similar spectral characteristics (422 nm Soret band of analogous intensity, broad α band) is observed. These observations suggest that in the Fe^{II}/Cu^{I} mixture of **1-(BArF)** and **2**, O_2 binding to iron(II) occurs first (further evidence is given below), but the presence of Cu subsequently affects the chemistry.

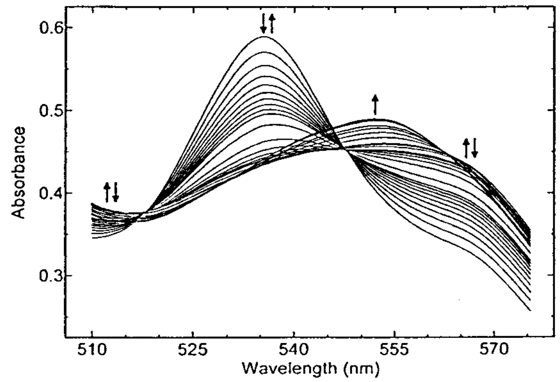

Figure 3. Experimental spectra (stopped-flow kinetic, 182 s total, −90 °C, acetone) for the reaction of O_2 with a 1:1 mixture of **1-(BArF)** and **2**. See text for further explanation.

Stopped-flow kinetics support this conclusion and provide additional insight. UV−vis spectral changes (α region only) are shown in Figure 3. At −90 °C in acetone, addition of O_2 to a 1:1 mixture of **1-(BArF)** and **2** results in the formation of a new species with λ_{max} = 535 nm, *within* the mixing time of the experiment (1 ms). This species corresponds to $(F_8TPP)Fe-O_2$, as described above (Scheme 2); this very fast formation is also observed when $(F_8TPP)Fe^{II}$ (**2**) independently is reacted with O_2 in a similarly weakly coordinating solvent, THF.[34] By contrast, the kinetics of oxygenation of **1-(BArF)** by itself in acetone show that its reaction with O_2 does not occur within the stopped-flow mixing time; the formation of the binuclear adduct, $[\{(MePY2)Cu\}_2(O_2)]^{2+}$, is relatively slow, with $\Delta H^‡ = -0.7 \pm 1$ kJ M^{-1}, $\Delta S^‡ = -164 \pm 4$ J K^{-1} M^{-1}, and no Cu/O_2 = 1:1 adduct is observed.[23] Thus, in mixtures of reactive iron(II) and copper(I) complexes, **1-(BArF)** and **2**, iron interacts with O_2 first.

Further, the low-temperature stopped-flow kinetic data reveal that, within 1 s, $(F_8TPP)Fe-O_2$ is transformed into a new species with a broad α-band absorption and with λ_{max} ~560 nm, perhaps similar to that obtained in the benchtop experiment for addition of O_2 to a 1:1 mixture of **1-(BArF)** and **2** in THF or acetone (vide supra). This further fast reaction shows two isosbestic points (518 and 548 nm; Figure 3); the corresponding second-order rate constant was determined to be $3.4 \pm 0.2 \times 10^4$ M^{-1} s^{-1}. An absorbance vs time plot is given in the Supporting Information. While further studies are clearly necessary, this reaction must represent an interaction of $(F_8TPP)Fe-O_2$ with **1-(BArF)**, perhaps producing a peroxo-bridged species.

The fast-forming product with broad λ_{max} ~560 nm absorption subsequently decays in a complicated manner (at least two relaxations) to the final product with λ_{max} = 552 nm, Figure 3. This product corresponds to our μ-oxo product complex, **5-(BArF)**. In the stopped-flow experiments, these latter reactions occur rather rapidly; **5-(BArF)** is formed to a significant extent within 3−5 min at −90 °C, which contrasts with our observations from the benchtop monitoring experiments described above, i.e., formation in hours. The explanation for these different reaction time scales appears to be the involvement of photochemistry, which is probably occurring in the stopped-flow experiments with a diode-array (unfiltered) light source. We have corroborated this assumption by carrying out our benchtop oxygenation experiments in the presence of additional light sources. In fact, when carrying out the reaction of a **1-(BArF)**/**2**/O_2 mixture (~−75 °C) and recording UV−vis spectra having an open shutter in a diode-array instrument, or by exposing the same mixture in a dewar cuvette assembly to a lightbulb, the rate of formation of **5-(BArF)** was significantly increased. We have previously noted strong photochemistry occurring with copper–dioxygen complexes employing ligands similar to MePY2,[35,36] while photolytic activity has been observed for cytochrome *c* oxidase O_2 intermediates[37] as well as O_2 adducts of other metal complexes.[38,39]

Further detailed stopped-flow kinetic studies or further investigations of the photochemistry which may be occurring here were not carried out. While the O_2 chemistry appears to be very rich, detailed analysis would be thwarted by the ever-present problem of not having exactly 1:1 ratios of iron(II) and copper(I) starting materials. Future inquiries may be directed at Fe···Cu complexes possessing binucleating ligands, such as L (see Introduction),[15] or analogues with tridentate tethers.[15c]

Protonation Titration. Formation of [(F_8TPP)Fe^{III}–(OH)–Cu^{II}(MePY2)](CF_3SO_3)$_2$ (6-(CF_3SO_3)$_2$). As shown in Scheme 1, the corresponding dicationic μ-hydroxo complex, **6-(CF_3SO_3)$_2$**, can also be prepared by two routes (Experimental Section). First, Et_3N is left out when reacting **3** and **4**. The second method is via the direct protonation of **5-(CF_3SO_3)**. Figure 3 shows the transformation of μ-oxo complex to **6-(CF_3SO_3)$_2$** via addition of increasing quantities of triflic acid, CF_3SO_3H. The 67.7 ppm pyrrole absorption (vide supra), converts to a new peak at 70.3 ppm. This further downfield shift suggests a weaker coupling in **6-(CF_3SO_3)$_2$** than in **5-(CF_3SO_3)**. This is also confirmed by comparison of the room-temperature magnetic moment of **6-(CF_3SO_3)$_2$** ($\mu_{eff} = 5.60\ \mu_B$; Evans NMR method). We can rule out that (F_8TPP)Fe^{III}–triflate is a product of the protonation, since it is known to have a pyrrole resonance at ~53 ppm.[13]

In the diamagnetic region, the "doublet" at 9.9 and 9.24 ppm, assigned to the *m*-phenyl porphyrinate resonances, also shifts to a new "doublet" at 11.54 and 10.73 ppm. By contrast, no significant shift of the 7.95 ppm *p*-phenyl absorption occurs upon conversion of **5-(CF_3SO_3)** to **6-(CF_3SO_3)$_2$**. This behavior observed for the *meso*-aryl groups was also seen in the protonation of [(F_8TPP)Fe–O–Cu(TMPA)]$^+$, which gave the μ-OH^- complex [(F_8TPP)Fe–OH–Cu(TMPA)]$^{2+}$.[13] The other peaks, which are associated with the protons of the MePY2 moiety, disappear during the protonation experiment (with 1 equiv of CF_3SO_3H) carried out at room temperature. We suggest that the relatively weaker M–(OH) bonds could result in partial dissociation of the iron and copper complex moieties within **6-(CF_3SO_3)$_2$**, in equilibrium with (F_8TPP)Fe–OH and **3-(CF_3SO_3)$_2$**. This supposition is consistent with the observation (vide infra) that the characteristic upfield-shifted peaks for the coupled $S = 2$ μ-hydroxo complex **6-(CF_3SO_3)$_2$** do appear when the temperature is lowered.

The protonation process is slow on the NMR scale, since two distinctive sets of resonances in mixtures of **5-(CF_3SO_3)** and **6-(CF_3SO_3)$_2$** are observed (Figure 4), rather than a single averaged peak which would be present if the exchange process were fast. A similar slow protonation was observed in the conversion of [(F_8TPP)Fe–O–Cu(TMPA)]$^+$ to [(F_8TPP)Fe–OH–Cu(TMPA)]$^{2+}$.[13] Slow protonation reactions seem to be a common feature for oxo-bridged metal ion species, e.g., bis(μ-oxo)–dimanganese(III)[40] and (μ-oxo)–diiron(III) com-

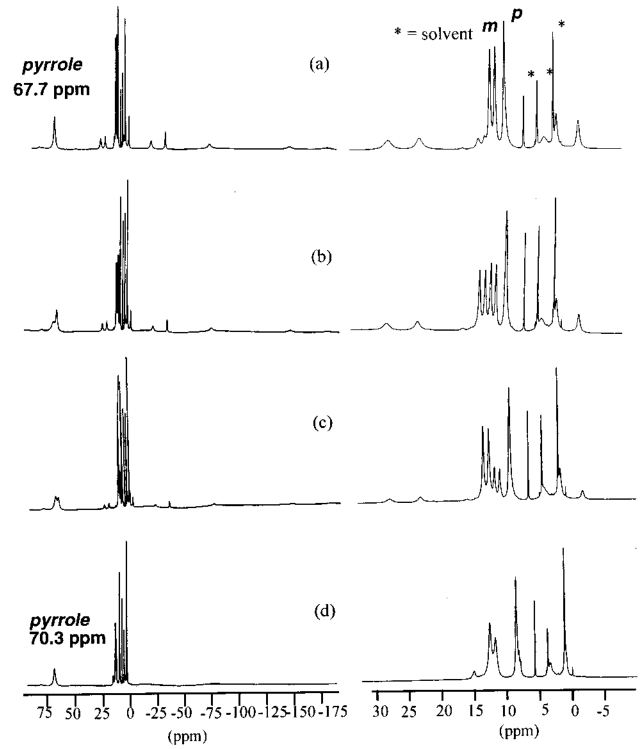

Figure 4. Addition of triflic acid to **5-(CF_3SO_3)** as followed by ^1H NMR spectroscopy (300 MHz, 297 K, CD_2Cl_2): (a) spectrum of **5-(CF_3SO_3)**, (b) after adding 0.33 equiv of CF_3SO_3H, (c) after adding 0.66 equiv of CF_3SO_3H, and (d) after adding 1 equiv of CF_3SO_3H, producing **6-(CF_3SO_3)$_2$**.

plexes.[41] Protonation usually results in bending of the previously near-linear M–O–M′ unit; the required rehybridization around the μ-oxo atom to give a M–(OH)–M′ product and concomitant structural rearrangements are generally seen to be the causes for the relatively slow proton-transfer reactions.[40,41]

The structure of **6-(CF_3SO_3)$_2$** has not been determined. On the basis of the apparent decrease in magnetic coupling (vide supra) of this complex compared to the parent μ-oxo complex **5-(CF_3SO_3)**, we propose that **6-(CF_3SO_3)$_2$** has a bent Fe–(OH)–Cu structure, as observed in [(F_8TPP)Fe–OH–Cu(TMPA)]$^{2+}$ ($\angle$Fe–OH–Cu ~ 157°).[13] We observe **6-(CF_3SO_3)$_2$** to be rather unstable and particularly moisture sensitive; for example, repeated attempts to obtain X-ray quality crystals invariably led to decomposition reactions yielding isolated species such as the μ-oxo diiron(III) complex [(F_8TPP)Fe^{III}–O–Fe^{III}(F_8TPP)]$^+$ and/or the bis-aquo complex [Cu^{II}(MePY2)(OH_2)$_2$](CF_3SO_3)$_2$.

Estimation of the pK_a of the Complex 6-(CF_3SO_3)$_2$. The protonation of complexes like **5-(CF_3SO_3)** is of general interest in the study of μ-oxo metal compounds[13,41,42] and is of possible importance in heme-copper oxidase function, since protons either are taken up to produce water from O_2 (scalar protons) or are translocated (vectorial protons).[3,13] In order to assess the pK_a of **6-(CF_3SO_3)$_2$**, we titrated **5-(CF_3SO_3)** with a variety of acids having known pK_a values in acetonitrile solvent (Table 2)[43] and monitored the formation of conjugate acid **6-(CF_3SO_3)$_2$** using ^1H NMR spectroscopy. A range of acids, from anilinium triflate (pK_a = 10.56) to trimethylammonium chloride (pK_a = 17.6 in CH_3CN), were used.

(35) Karlin, K. D.; Nasir, M. S.; Cohen, B. I.; Cruse, R. W.; Kaderli, S.; Zuberbühler, A. D. *J. Am. Chem. Soc.* **1994**, *116*, 1324–1336.
(36) Karlin, K. D.; Wei, N.; Jung, B.; Kaderli, S.; Niklaus, P.; Zuberbühler, A. D. *J. Am. Chem. Soc.* **1993**, *115*, 9506–9514.
(37) Varotsis, C. A.; Babcock, G. T. *J. Am. Chem. Soc.* **1995**, *117*, 11260–11269.
(38) MacArthur, R.; Sucheta, A.; Chong, F. F. S.; Einarsdóttir, O. *Proc. Natl. Acad. Sci. U.S.A.* **1995**, *92*, 8105–8109.
(39) Maeder, M.; Mäcke, H. R. *Inorg. Chem.* **1994**, *33*, 3135–3140.
(40) Carroll, J. M.; Norton, J. R. *J. Am. Chem. Soc.* **1992**, *114*, 8744–8745.
(41) Kramarz, K. W.; Norton, J. R. *Prog. Inorg. Chem.* **1994**, *42*, 1–65.
(42) Evans, D. R.; Mathur, R. S.; Heerwegh, K.; Reed, C. A.; Xie, Z. *Angew. Chem., Int. Ed. Engl.* **1997**, *36*, 1335–1337.

Table 2. Protonation of **5** by Different Acids

Proton source	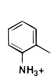	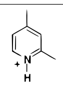	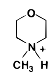	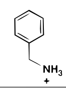	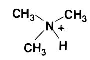
pKa (CH_3CN)[37]	10.56	14.0	15.59	16.76	17.6
Protonation ?	Yes	Yes	Yes	Yes	No
product	μ-OH	μ-OH	μ–OH	low-spin Fe(III)	

Addition of 1 equiv of trimethylammonium triflate does not cause protonation of **5-(CF_3SO_3)**. However, a complete and clean conversion of **5-(CF_3SO_3)** to **6-(CF_3SO_3)$_2$** occurs when *N*-methylmorpholinium triflate and 2,4-lutidinium triflate are used. The protonation of the μ-oxo complex has also been observed with benzylammonium triflate and the stronger protic acid anilinium triflate, Table 2. In these latter cases, a second set of peaks, typical of a low-spin Fe(III) porphyrin, was observed at 23 and −20 ppm. This behavior indicates that these sterically nonhindered ammonium salts first protonated the μ-oxo bridge and the hydroxo complex formed reacted immediately with the liberated amine (conjugate base) to give the low-spin species product. We can conclude that the pK_a of **6-(CF_3SO_3)$_2$** is 16.7 < pK_a < 17.6. It has been suggested by Pecoraro et al.[43a] that the corresponding aqueous pK_a would be 7.5 ± 1 pK_a units lower than in CH_3CN, meaning we can estimate a pK_a for **6-(CF_3SO_3)$_2$** in water of 9.6 ± 2. Clearly, the oxo moiety in **5-(CF_3SO_3)** is quite basic and the pK_a is very comparable to that observed in our study of μ-oxo complex [(F_8-TPP)Fe−O−Cu(TMPA)]$^+$ (pK_a (H_2O), 8 ± 2.5). In contrast, other known oxo-bridged Fe, Mn, and Ru complexes have pK_a values below this range.[43a,44,45] For instance, the pK_a value for [$(HBpz_3)_2Fe_2(OH)(O_2CCH_3)_2$]$^+$ [$HBpz_3$ = hydrotris(1-pyrazolyl)borate] and [(L′)Ru(OH)(O_2CCH_3)$_2$Fe(L″)]$^{3+}$ (L′ = 1,4,7-triazacyclononane, L″ = 1,4,7-trimethyl-1,4,7-triazacyclononane) are estimated to be around 3.5.[44] Oxo-bridged manganese complexes, [$Mn^{IV}(\mu\text{-O})_n(\mu\text{-OH})]_2^+$ (n = 1[43a] or 2[45]), have aqueous pK_a values around −2 < pK_a (H_2O) < 7. The lower pK_a value in these Fe^{III}−O−Cu^{II} complexes may be due to the presence of copper(II), thus a metal with a lower oxidation state (and therefore decreased Lewis acidity) compared to the metals (Fe, Ru, Mn) in the complexes mentioned above.

Variable-Temperature (VT) NMR Studies. As expected for a paramagnetic system, the proton resonances in **5-(CF_3SO_3)** exhibit a strong temperature dependence. Variable-temperature ^{1}H NMR data have been obtained, and these, along with plots of chemical shift versus 1/T (Curie plots) for the temperature range 293−213 K, are given in the Supporting Information. No dramatic changes in the diamagnetic region are observed when the temperature is lowered. However, the upfield-shifted signals move further upfield while the downfield signals move further downfield, all with broadening. The δ vs 1/T plots show linear Curie and anti-Curie behavior, consistent with a strong antiferromagnetic coupling dominated by a single spin state in the temperature range studied.[14] The MePY2 proton upfield-shifted signals, all except one, have associated positive (i.e., downfield) extrapolated intercepts, consistent with the breaking of the strong antiferromagnetic coupling as T approaches infinity; theoretically, the system uncouples to behave as a Cu(II) mononuclear species.

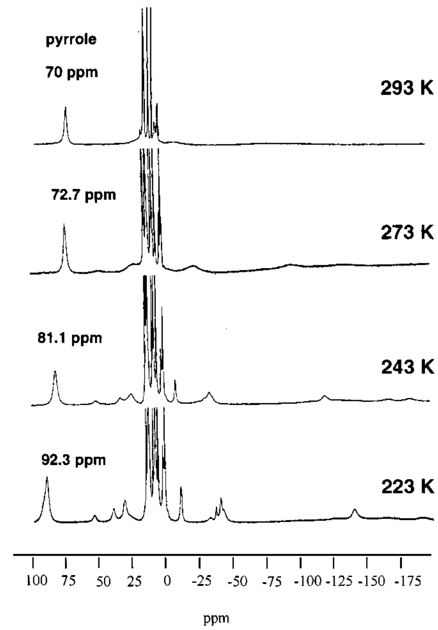

Figure 5. Variable-temperature ^{1}H NMR spectra (300 MHz, CD_2Cl_2) of **6-(CF_3SO_3)$_2$**. Curie plots are given in the Supporting Information.

Figure 5 shows the effect of lowering the temperature on ^{1}H NMR spectra of the μ-hydroxo-bridged complex **6-(CF_3SO_3)$_2$**. Resonances, which might be assignable to the MePY2 ligand, are not seen at room temperature. However, upon cooling, these peaks do appear, and they exhibit a profile rather similar to that observed for the μ-oxo analogue **5-(CF_3SO_3)**. Along with the observed magnetic moment of **6-(CF_3SO_3)$_2$** (vide supra), the behavior is what is expected for the postulated S = 2 antiferromagnetically coupled system. The behavior (i.e., the lack of signals at room temperature) must be ascribed to the presence of the μ-OH^- rather than μ-oxo ligand. The same phenomenon was also observed for [(F_8TPP)Fe^{III}−OH−Cu^{II}-(TMPA)]$^{2+}$, in comparison to [(F_8TPP)Fe^{III}−O−Cu^{II}(TMPA)]$^+$. As proposed and discussed for this TMPA analogue set of compounds,[14] the weaker M−(OH) bonds allow for relatively rapid ligand exchange phenomena near room temperature, leading to line broadening.

Summary and Conclusion

The following are the principal results and conclusions of this investigation:

The oxo-bridged heme-copper assembly [(F_8TPP)Fe−O−Cu(MePY2)]$^+$ (**5**) is readily prepared in good yield by acid−base self-assembly, using [(MePY2)Cu^{II}](CF_3SO_3)$_2$ (**3-(CF_3SO_3)$_2$**) and the hydroxo species [(F_8TPP)Fe^{III}−OH] (**4**) in the presence of a suitable base. This μ-oxo Fe^{III}−O−Cu^{II} complex has been characterized by techniques including UV−vis, multinuclear NMR, and IR spectroscopies, magnetism, and solution conductivity. Its ^{1}H NMR spectrum has been assigned by specific deuteration of the porphyrinate moiety as well as the MePY2 ligand and reveals the presence of an antiferromagnetic coupling between the high-spin Fe(III) (S = 5/2) and Cu(II) (S = 1/2) ions, to give an S = 2 spin system. Room-temperature magnetic moment measurements corroborate the S = 2 assignment for **5-(CF_3SO_3)**.

We have shown that **5-(BArf)** could also be prepared by O_2 reaction with [(MePY2)Cu^I(CH_3CN)](BArF) (**1-(BArF)**) and

(43) (a) Baldwin, M. J.; Gelasco, A.; Pecoraro, V. L. *Photosynth. Res.* **1993**, *38*, 303−308 and references cited therein. (b) Izutsu, K. *Acid-Base Dissociation Constants in Dipolar Aprotic Solvents*; Blackwell Scientific Publications: Boston, 1990.
(44) Turowski, P. N.; Armstrong, W. H.; Liu, S.; Brown, S. N.; Lippard, S. J. *Inorg. Chem.* **1994**, *33*, 636−645 and references cited therein.
(45) Hage, R.; Krijnen, B.; Warnaar, J. B.; Hartl, F.; Stufkens, D. J.; Snoeck, T. L. *Inorg. Chem.* **1995**, *34*, 4973−4978.

$(F_8TPP)Fe^{II}$ (**2**). Low-temperature stopped-flow kinetics reveals the presence of rapidly forming intermediates, including a 1:1 adduct $(F_8TPP)Fe-O_2$, which forms first, even in the presence of **1**; the species observed subsequently requires the presence of Cu and is tentatively assigned as a peroxo-bridged species. The μ-oxo final product **5-(BArF)** forms in a slower process.

We have also established the acid−base interconversion of $[(F_8TPP)Fe-O-Cu(MePY2)](CF_3SO_3)$ (**5-(CF$_3$SO$_3$)**) to $[(F_8TPP)Fe-(OH)-Cu(MePY2)](CF_3SO_3)_2$ (**6-(CF$_3$SO$_3$)$_2$**) by synthetic chemistry, and through protonation of the oxo ligand as followed in a ^{1}H NMR titration. The physical properties of **5-(CF$_3$SO$_3$)** and **6-(CF$_3$SO$_3$)$_2$** have been compared. The oxo group in **5-(CF$_3$SO$_3$)** is more basic than most of the known oxo-bridged metallic systems, but is similar to the previously studied μ-oxo complex $[(F_8TPP)Fe^{III}-O-Cu^{II}(TMPA)]^+$. The aqueous p$K_a$ of **6-(CF$_3$SO$_3$)$_2$** is estimated to be 9.6 ± 2.

The observed room-temperature and variable-temperature ^{1}H NMR chemical shifts of **5-(CF$_3$SO$_3$)** and **6-(CF$_3$SO$_3$)$_2$** are consistent with the presence of a predominant σ contact shift mechanism. Linear Curie plots of the respective pyrrole and MePY2 chemical shifts are consistent with a pure spin state, in each case $S = 2$. The lack of signals at room temperature for the MePY2 moiety in **6-(CF$_3$SO$_3$)$_2$** must be ascribed to the presence of the μ-OH$^-$ rather than μ-oxo ligand; the weaker M−(OH) bonds allow for relatively rapid ligand exchange phenomena near room temperature, leading to line broadening.

Complexes **5** and **6** are comparable in composition and physical properties (especially, magnetic and paramagnetically shifted NMR spectra) to the previously studied TMPA analogues, $[(F_8TPP)Fe^{III}-O-Cu^{II}(TMPA)]^+$ and $[(F_8TPP)Fe^{III}-OH-Cu^{II}(TMPA)]^{2+}$.[13,14] While detailed structural insights for **5** and **6** are currently unavailable, one can anticipate very similar near-linear μ-oxo and bent μ-hydroxo cores, respectively, to be present. Thus, as previously discussed,[13] **5** and, especially, **6** may represent structural models for the oxidized $Fe^{III}-X-Cu^{II}$ resting state, or turnover intermediates, in heme-copper oxidases.

Experimental Section

Reagents and solvents used were of commercially available analytical reagent quality, and all chemicals were obtained from Aldrich Chemical Co. unless otherwise noted. Diethyl ether (Et_2O), tetrahydrofuran (THF), and heptane were distilled over sodium/benzophenone ketyl under an argon atmosphere. Acetonitrile (CH_3CN) was distilled from CaH_2. Acetone ($CH_3C(O)CH_3$) was shaken with Drierite for several hours before it was decanted and distilled from fresh Drierite under argon. Dichloromethane (CH_2Cl_2) was stirred with concentrated sulfuric acid for several days and washed with water, sodium carbonate (10%) solution, and water. It was then dried over anhydrous magnesium sulfate, filtered, and predried over CaH_2 before a final distillation over fresh CaH_2 under an argon atmosphere. Triethylamine (Et_3N) was first dried with KOH and then distilled from CaH_2. Preparation and handling of air-sensitive materials were carried out under an argon atmosphere with use of standard Schlenk techniques. Deoxygenation of solvents and solutions was effected either by repeated vacuum/purge cycles using argon (freeze−pump−thaw) or through bubbling of Ar directly through the solutions. Solid samples were stored and transferred, and samples for IR, UV−vis, and NMR spectra were prepared in Vacuum Atmospheres Co. and/or MBraun Co. dryboxes filled with prepurified nitrogen. Elemental analyses were performed by Desert Analytics, Tucson, AZ. Infrared spectra were recorded as Nujol mulls on a Mattson Galaxy 4030 FT-IR spectrometer driven by a Dell Dimension P133 computer using software written by Mattson. Melting points were determined on a Mel Temp II, Laboratory Devices. UV−visible spectra were recorded on a Shimadzu 160 spectrophotometer or a Hewlett-Packard 8452A diode-array spectrophotometer driven by a Gateway 2000 P75 computer using software written by On-Line Instruments Systems, Inc. ^{1}H, ^{2}H, and ^{19}F NMR spectra were recorded on a Bruker NMR instrument at 300 MHz or on a Varian NMR instrument at 400 MHz. Chemical shifts are reported as δ values, downfield from an internal standard (Me_4Si) (^{1}H), as δ values referenced to solvent (^{2}H), or as δ values referenced to an external standard of α,α,α-trifluorotoluene (^{19}F). EI/CI and FAB-MS spectra were recorded at the University of Illinois, Urbana-Champaign.

F$_2$dp, (2,6-Difluorophenyl)dipyrromethane. A solution of 2,6-difluorobenzaldehyde (5 g, 35.2 mmol) in 100 mL of freshly distilled pyrrole was stirred and degassed for 15 min with a stream of argon. Then, 0.5 mL of trifluoroacetic acid was added dropwise anaerobically. The resulting red mixture was stirred for an additional 1 h. Then 100 mL of ACS-grade dichloromethane was added. The organic layer was washed three times with 75 mL of 0.1 M NaOH and dried over anhydrous $MgSO_4$. Dichloromethane was distilled off using a rotary evaporator while excess pyrrole was distilled off under high vacuum. A greenish paste was obtained and was chromatographed over silica using 4:1 hexane/diethyl ether containing 1% triethylamine. A red (third, over Br_2, $R_f = 0.3$) fraction was collected. This fraction was crystallized in a mixture of hexane/ether (10:1) to yield white needles (4.1 g, 45%). ^{1}H NMR ($CDCl_3$): 8.17 (s, br, 2H, N−H pyrrole), 7.16−7.26 (m, 1H, para phenyl), 6.87−6.93 (t, 2H, meta phenyl), 6.68−6.70 (m, 2H, γ pyrrole), 6.13−6.15 (q, 2H, α pyrrole), 6.01 (s, 2H, β pyrrole), 5.91 (s, 1H, CH).

F$_8$TPPH$_2$, Tetrakis(2,6-difluorophenyl)porphyrin. In a 1 L two-necked round-bottom flask, 4 g (15.5 mmol) of 2,6-difluorodipyrromethane and 2.2 g (15.5 mmol, 1 equiv) of 2,6-difluorobenzaldehyde were mixed with 1 mL of boron trifluoride−diethyl etherate ($BF_3 \cdot Et_2O$) in 750 mL of freshly distilled dichloromethane. The orange solution was stirred for 2 h. During this time, the color changed from initial yellow orange through red to purple. Formation of porphyrinogen (λ_{max} = 500 nm) was monitored using optical spectra. Then, 6.15 g (27.1 mmol, 3.5 equiv) of 2,3-dichloro-5,6-dicyanobenzoquinone (DDQ) was introduced to oxidize the solution. The mixture was stirred for 8 h. The volume was reduced and the reaction mixture further purified first by flash chromatography over basic Al_2O_3 eluted with CH_2Cl_2 and then by column chromatography (silica, 2% methanol in CH_2Cl_2) to afford 3 g of F_8TPPH_2. R_f (alumina, CH_2Cl_2) = 0.85. ^{1}H NMR ($CDCl_3$, 300 MHz): δ 8.8 (m, 8H, pyrrole H), 7.74 (d, 4H, para phenyl H), 7.31 (m, 8H, meta phenyl H).

F$_8$TPPH$_2$-*d*$_8$. The pyrrole-deuterated F_8TPPH_2-d_8 tetrakis(2,6-difluorophenyl)porphyrin was prepared by modification of the standard benzaldehyde−pyrrole condensation in propionic acid/nitrobenzene reflux, as previously reported in the literature.[46] To a 1 L two-necked round-bottom flask were added 500 mL of propionic anhydride (97%) and 72 mL of D_2O (99.9 atom % D) under argon, and the solution was brought to reflux for 1 h. Under argon, 6.0 g pyrrole was added to this deuterated propionic acid, and the reaction mixture was refluxed for an additional 1 h. In air, 125 mL of nitrobenzene and 12.5 g of 2,6-difluorobenzaldehyde were added. Reflux continued for 1 h, after which the reaction mixture was cooled to room temperature and placed in a freezer (−20 °C) for 2 days. The resulting purple solid was collected via filtration over Celite, washed with water (1 L), dried over air, and removed from Celite with CH_2Cl_2 (1 L). The solution was dried over $MgSO_4$, filtered, and concentrated to dryness via rotary evaporation. The crude material was first purified over an alumina column using methylene chloride (R_f = 0.85) eluent, and then purified further over a silica column with 50:50 CH_2Cl_2/hexane to afford 1.3 g of purple solid. ^{1}H NMR ($CDCl_3$, 300 MHz): δ 7.75 (d, 4H, para phenyl H), 7.30 (m, 8H, meta phenyl H).

(F$_8$TPP)Fe^{III}OH (4) and (F$_8$TPP-*d*$_8$)Fe^{III}OH were synthesized according to published procedures.[12]

(F$_8$TPP)Fe^{III}OH. ^{1}H NMR ($CDCl_3$): δ 81.1 (v br, 8H, pyrrole H), 11.5, 10.5 (d, 8H, meta phenyl), 7.3 (s, 4H, para phenyl). UV−vis (CH_2Cl_2): 408 (Soret), 572 nm.

(F$_8$TPP)Fe^{II} (2). In a 100 mL Schlenk flask, 500 mg (0.6 mmol) of $(F_8TPP)Fe^{III}OH$ was dissolved in Ar-saturated CH_2Cl_2 (ca. 50 mL), and

(46) (a) Adler, A. D.; Longo, F. R.; Kampas, F.; Kim, J. *J. Inorg. Nucl. Chem.* **1970**, 32. (b) Adler, A. D.; Longo, F. R.; Finarelli, J.; Goldmacher, J.; Assour, J.; Korsakoff, L. *J. Org. Chem.* **1967**, *32*, 476.

to it was added a 1 M aqueous solution (ca. 30 mL) of sodium hydrosulfite (Ar-saturated) under argon. The two solutions were mixed vigorously for about 30 min. The color of the reaction mixture changed from brown to bright red. The two layers were separated, and the organic layer was dried over $MgSO_4$ (under Ar). The solvent was concentrated in vacuo, and addition of deoxygenated heptane (ca. 50 mL) precipitated **2** as a purplish solid (350 mg, 72%). Anal. Calcd for $C_{44}H_{20}N_4F_8Fe{\cdot}H_2O$: C, 63.63; H, 2.67; N, 6.75; F, 18.3. Found: C, 63.78; H, 2.35; N, 6.84; F, 18.9. ^{1}H NMR (acetone-d_6, 300 MHz): δ 48.71 (s, 8H, pyrrole H), 7.72 (s, 4H, para phenyl H), 7.20−7.38 (d, 8H, meta phenyl H). UV−vis (acetone): 421 nm, 545 nm.

Vinylpyridine-d_2 ($C_4H_4NCH{=}CD_2$). To a 100 mL Schlenk flask was introduced (methyl-d_3)triphenylphosphonium iodide (4.5 g, 11.05 mmol). The solid was suspended with freshly distilled THF (30 mL) and cooled to 0 °C. *n*-BuLi (2.5 M in hexane, 4.65 mL, 1.04 equiv) was added to the suspension at 0 °C, via a syringe. The resulting deep orange mixture was stirred for 15 min at 0 °C and allowed to warm to room temperature. To this solution was added a solution of 2-pyridinecarboxaldehyde (1.18 g, 1 equiv) in 50 mL of THF under argon. After stirring at room temperature for 18 h, the solution was filtered and the solvent was evaporated under reduced pressure. The resulting reddish oil was purified by column chromatography (silica, 40% ethyl acetate in hexane) to afford 350 mg of product (30% yield). ^{1}H NMR ($CDCl_3$, 300 MHz): δ 8.51 (d, 1H, pyridyl H6), 7.58 (td, 1H, pyridyl H4), 7.28 (d, 1H, pyridyl H3), 7.05 (m, 1H, pyridyl H5), 6.7 (brs, 1H, CH═). ^{2}H NMR ($CDCl_3$, 400 MHz): δ 6.10 (D cis), 5.4 (D trans).

***N*-(Methyl-d_3)-*N*-[2-(2-pyridinyl)(ethyl-d_2)]-2-pyridine(ethane-d_2)-amine, $CD_3N(CH_2CD_2PY)_2$, MePY2-d_7.** 2-Vinylpyridine (483 mg, 4.6 mmol) and methylamine-d_5 deuteriochloride (112 mg, 1.53 mmol) were placed in a 10 mL round-bottom flask. The reactants were stirred under reflux in 3 mL of D_2O and 200 mL of CD_3OD for 16 h. After cooling, the methanol was removed and the resulting mixture was washed with 1 N NaOH solution (ca. 10 mL) and extracted with CH_2Cl_2. The organic layer was dried over $MgSO_4$ and purified by column chromatography (alumina, 2% MeOH in ethyl acetate) to afford 175 mg of MePY2-d_7 (yield 45%). ^{1}H NMR ($CDCl_3$, 300 MHz): δ 8.33 (d, 2H, pyridyl H6), 7.38 (t, 2H, pyridyl H4), 6.95 (d, 2H, pyridyl H3), 6.91 (t, 1H, pyridyl H5), 2.67 (s, 4H, CH═). ^{2}H NMR ($CDCl_3$, 400 MHz): δ 3.165 (br s, $-CD_2-$PY), 2.5 (br s, $-CD_3$).

***N*-(Methyl-d_3)-*N*-[2-(2-pyridinyl)(ethyl-d_4)]-2-pyridine(ethane-d_4)-amine, $CD_3N(CD_2CD_2PY)_2$, MePY2-d_{11}.** The same procedure as the one described for MePY2-d_7 was used, starting with the deuterated d_2-2-vinylpyridine. ^{1}H NMR ($CDCl_3$, 300 MHz): δ 8.45 (d, 2H, pyridyl H6), 7.50 (t, 2H, pyridyl H4), 7.07 (d, 2H, pyridyl H3), 7.05 (t, 1H, pyridyl H5). ^{2}H NMR ($CDCl_3$, 400 MHz): δ 2.995 (m, $-CD_2-CD_2-$), 2.518 (brs, CD_3).

[(MePY2)Cu^{II}](CF_3SO_3)$_2$, 3-(CF_3SO_3)$_2$. To a solution of Cu^{II}(CF_3SO_3)$_2$ (2 g, 5.5 mmol) in MeOH (20 mL) under a stream of argon was added a solution of deoxygenated MePY2 (1.33 g, 5.5 mmol, 1 equiv) dropwise, and the resulting blue mixture was stirred for 1 h. The solvent was then evaporated, and freshly distilled air-free diethyl ether was added. The resulting precipitate was filtered off, washed several times with diethyl ether, and dried in vacuo to give [(MePY2)Cu^{II}](CF_3SO_3)$_2$ as a blue solid (2.9 g, 87%). Anal. Calcd for $C_{17}H_{19}N_3CuF_6S_2O_6$: C, 33.86; H, 3.18; N, 6.97; S, 10.63. Found: C, 33.90; H, 3.07; N, 6.76; S, 10.25.

[(MePY2)Cu(I)(CH_3CN)](BArF), 1-(BArF). To a flame-dried 100 mL Schlenk flask were transferred anaerobically 0.5 g (0.56 mmol) of sodium tetrakis[(3,5)-bis(trifluoromethyl)phenyl]borate (NaBArF), 280 mg (1.5 equiv, 0.85 mmol) of copper(I) tetrakisacetonitrile perchlorate ([Cu(CH_3CN)$_4$](ClO_4)), and an oven-dried spin bar. Then 30 mL of degassed freshly distilled dry diethyl ether was added. The beige mixture was stirred for 30 min and then filtered into another Schlenk flask to remove the excess of [Cu(CH_3CN)$_4$](ClO_4). After reduction of the solvent volume (in vacuo), addition of deoxygenated dry heptane gave 450 mg of a white microcrystalline material (73%). Then 100 mg (0.415 mmol) of vacuum-dried MePY2 was dissolved in 25 mL of freshly distilled diethyl ether. The yellow solution was introduced anaerobically into the Schlenk flask containing the [Cu(CH_3CN)$_4$](BArF). The bright yellow mixture was stirred for 30 min and then filtered into a 250 mL Schlenk flask. The yellow solution was concentrated before being layered with 100 mL of anhydrous heptane. A pale yellow solid was collected after several hours, washed several times with heptane, and dried in vacuo to afford 425 mg of yellow solid (yield 85%). Anal. Calcd for ($C_{47}H_{31}N_3F_{31}BCu$)·CH_3CN: C, 48.67; H, 2.83; N, 4.63. Found: C, 48.77; H, 2.72; N, 4.62. The presence of acetonitrile has been confirmed by ^{1}H NMR. ^{1}H NMR (CD_3NO_2, 300 MHz): δ 8.65 (d, 2H, *o*-PY), 7.88 (t, 2H, *p*-PY), 7.85 (s br, 8H, BArF-H$_2$), 7.66 (s, 4H, BArF-H4), 7.41 (m, 4H, *m*-PY), 3.06 (br, 8H, $-CH_2-$PY), 2.50 (br, 3H, $N-CH_3$), 2.10 (s, 3H, CH_3CN). IR (Nujol, cm^{-1}): 1611 (s, br, C═C), 1573 (w, C═C) 1115 (s, br, BArF).

[(F_8TPP)Fe−O−Cu(MePY2)](CF_3SO_3), 5-(CF_3SO_3). In a 100 mL Schlenk flask equipped with a stir bar were charged 215 mg (0.259 mmol) of (F_8TPP)Fe^{III}OH and 156 mg (0.259 mmol) of [(MePY2)-Cu^{II}](CF_3SO_3)$_2$. These were stirred for 30 min to effect intimate mixing. Then deaerated THF or CH_3CN (10 mL) was introduced. A brownish-red solution was generated, to which was promptly added Et_3N (36 μL, 1 equiv), via a syringe. The resulting red solution was stirred for an 1 h and then layered with diethyl ether. The precipitate was filtered off on a coarse frit and dried in vacuo for 24 h to give 220 mg of black microcrystalline product (66% yield). Anal. Calcd for ($C_{60}H_{39}N_7F_{11}$-SO_4CuFe)·2H_2O: C, 54.64; H, 3.26; N, 7.438; S, 2.42. Found: C, 54.23; H, 3.02; N, 7.34; S, 2.36. The presence of H_2O was confirmed by examination of the ^{1}H NMR spectrum. ^{1}H NMR (CD_2Cl_2): δ 67.7 (s, 8H, pyrrole), 23.4−18.9 (d, 4H, $-CH_2-$PY), 9.90−9.24 (d, 8H, *m*-phenyl), 7.95 (s, 4H, *p*-phenyl), 1.2, −2.7, −23.5, and −37.2 (4 s, 4 2H, pyridyl hydrogens), −87.7 and −155.4 (2 s, 2 2H, $N-CH_2$), −189.4 (brs, 3H, $N-CH_3$). ^{19}F NMR (CH_2Cl_2): δ −78.74 (s, $CF_3SO_3^-$), −95.87 and −96.71 (d, fluorine F_8TPP). UV−visible (CH_2Cl_2): 443, 555 nm.

The same procedure was used to prepare the following complexes.

[(F_8TPP-d_8)Fe−O−Cu(MePY2)](CF_3SO_3). ^{2}H NMR (CH_2Cl_2): δ 66.36 (s, D-pyrrole).

[(F_8TPP)Fe−O−Cu(CD_3N)(CH_2CD_2PY)$_2$](CF_3SO_3). ^{2}H NMR (CH_2Cl_2): δ 23.75−19.61 (d, $-CD_2-$PY), −182.76 (s, $-CD_3$).

[(F_8TPP)Fe−O−Cu(CD_3N)(CD_2CD_2PY)$_2$](CF_3SO_3). ^{2}H NMR (CH_2Cl_2): δ 24.26−20.20 (d, $-CD_2-$PY), −75.78 and − 149 ($-CD_2-$N), −182.76 (s, $-CD_3$).

[(F_8TPP)Fe−O−Cu(MePY2)](BArF), 5-(BArF). In a 100 mL Schlenk flask equipped with a stir bar were placed, in the drybox, 210 mg (0.2 mmol) of (F_8TPP)Fe^{II} and 302 mg (0.2 mmol, 1 equiv) of [(MePY2)Cu^I(CH_3CN)](BArF), to which was added air-free freshly distilled THF (20 mL). The reaction mixture was cooled to − 78 °C (dry ice−acetone bath) and stirred for 30 min. The solution was subjected to three cycles of vacuum/O_2 purging (O_2; UHP, Aldrich). The solution was finally allowed to warm slowly at room temperature and layered with 80 mL of deoxygenated heptane. After 5 h, the solution was filtered and the black microcrystalline solid dried in vacuo (330 mg, 65% yield). Anal. Calcd for ($C_{91}H_{51}N_7F_{31}$BOCuFe)·H_2O: C, 54.77; H, 2.68; N, 4.91. Found: C, 54.39; H, 2.4; N, 4.93. ^{1}H NMR (CD_2Cl_2): δ 67.6 (s, 8H, pyrrole), 24.01−20.53 (d, 4H, $-CH_2-$PY), 9.8−9.14 (d, 8H, *m*-phenyl), 7.67−7.51 (m, 16H, 8H BArF + *p*-phenyl), −84.4 and −147.4 (2 s, 2 2H, $-CH_2-$N), −177.1 (brs, 3H, $-CH_3$).

[(F_8TPP)Fe−OH−Cu(MePY2)](CF_3SO_3)$_2$, 6-(CF_3SO_3)$_2$. In a 100 mL Schlenk flask equipped with a stir bar were charged 200 mg (0.241 mmol) of (F_8TPP)Fe^{III}OH and 145 mg (0.241 mmol) of [(MePY2)-Cu^{II}](CF_3SO_3)$_2$. These were stirred for 30 min to effect intimate mixing. Then deaerated CH_3CN (7.5 mL) was introduced. A brownish-red solution was generated and stirred at room temperature for 1 h. The solution was then layered with toluene and allowed to stay at −20 °C for several hours. The black precipitate was filtered off on a coarse frit and dried in vacuo for 24 h to give 275 mg of black microcrystalline product (80% yield). Anal. Calcd for ($C_{61}H_{40}N_7F_{14}S_2O_7$CuFe)·2$H_2O$: C, 49.89; H, 3.02; N, 6.68. Found: C, 49.34; H, 3.16; N, 6.32. The presence of H_2O was confirmed by examination of the ^{1}H NMR spectrum. ^{1}H NMR (CD_2Cl_2, 300 MHz, 297 K): δ 70.3 (s, 8H, pyrrole), 11.54−10.73 (d, 8H, *m*-phenyl), 7.95 (s, 4H, *p*-phenyl).

NMR Titration. Protonation of 5-(CF_3SO_3). In the glovebox, a solution of **5-(CF_3SO_3)** (30 mg, 0.0234 mmol) in CD_2Cl_2 was prepared and transferred to an NMR tube, and the ^{1}H NMR spectrum was recorded. CF_3SO_3H (0.4 μL, 4.68 × 10^{-6} mol, 0.2 equiv), from a freshly opened vial from Aldrich, was then introduced via a 1 μL syringe, and the ^{1}H NMR spectrum was recorded. This process of adding aliquots of acid and recording spectra was performed several times until the titration "end-point" was reached. The same procedure was used for the pK_a determination, using the appropriate acid (see below).

pK_a Determination. General Preparation of the Protonated Amines. In a 25 mL round-bottom flask containing 10 mL of absolute ethanol was placed 5 mmol of the corresponding amine (i.e., aniline, 2,4-lutidine, methylmorpholine, and so on). To the solution was added 1 equiv of triflic acid, and the mixture was stirred for an additionnal 30 min. The volume of ethanol was reduced to 1 mL, and ~15−20 mL of diethyl ether was added. After 1 or 2 h, a white crystalline solid was filtered on a coarse frit and dried in vacuo for 12 h. ^{1}H NMR ($CDCl_3$ + 1 drop of d_6-DMSO).

Methylmorpholinium triflate: δ 9.56 (s br, 1H, NH^+), 3.95 (d, 2H, $-CH_2-$), 3.75 (t, 2H, $-CH_2-$), 3.44 (d, 2H, $-CH_2-$), 3.01 (t, 2H, $-CH_2-$), and 2.9 (s, 3H, $-CH_3$). Mp: 92.5 °C.

Anilinium triflate: δ 9.8 (v br, 3H, NH_3^+), 7.37 (m, 4H, H aromatic). Mp: 268 °C.

2,4-Lutidinium triflate: δ 15.13 (s br, 1H, NH^+), 8.6 (d, 1H, H ortho), 7.714 (d, 1H, meta) 7.65 (s, 1H, meta), 2.58 (s, 3H, $-CH_3$), and 2.47 (s, 3H, $-CH_3$). Mp: 62.5 °C.

Benzylammonium triflate: δ 6.96 (s br, 3H, NH_3^+), 6.31−6.22 (m, 5H, H aromatic), and 2.899 (s, 2H, $-CH_2$). Mp: 175.5 °C.

Magnetic Susceptibility Measurements. Room-temperature solid magnetic moments were determined with the use of a Johnson Matthey magnetic susceptibility balance calibrated against $Hg[Co(SCN)_4)]$. Solution magnetic moment measurements were conducted using the Evans method[47] on a Bruker NMR instrument at 300 MHz. To this end, samples with known concentration were made up in CD_2Cl_2. From the downfield shift of the TMS signal, with respect to that from the capillary reference tube, the paramagnetic susceptibility χ'_m was calculated using the following formula: $\chi'_m = (-3/4\pi)(\Delta\nu/\nu)(1000/c) + (\chi_0 M_w) - \chi_D$, where $\Delta\nu$ is the difference in shift of the reference signal in hertz, ν is the spectrometer frequency, c is the concentration of the complex in moles per liter, χ_0 is the solvent susceptibility, M_w is the molecular weight of the complex, and χ_D is the diamagnetic contribution to susceptibility. The latter was calculated using tabulated Pascal's constants.[48] The magnetic moment μ_{eff} is derived from the following formula: $\mu_{eff} = 2.84\sqrt{(\chi'_m T)}\mu_B$.

Electrical Conductivity. Electrical conductivity measurements were carried out in CH_3CN with a Barnstead model PM-70CB conductivity bridge and YSI model 3403 conductivity cell. The cell constant was determined with a standard aqueous solution of KCl (0.1 M). The molar conductivity, Λ_m, of a solution of **5-(CF_3SO_3)** was determined from the expression $\Lambda_m = 1000K/C_m$, where K is the cell constant divided by the measured resistance and C_m is the molar concentration of the solute (~10^{-3} M). Λ_m (CH_3CN) = 154 Ω cm^2 mol^{-1}, corresponding to a 1:1 electrolyte.[26]

Stopped-Flow Kinetics. The instrumentation and methods for analysis were as previously described.[35,36] Here, seven runs at −90 °C in acetone (Uvasol, Fluka) were carried out, with 2.75 × 10^{-4} M **1-(BArF)** and 2.73 × 10^{-4} M **2**; [O_2] = 5.92 × 10^{-3} M.

Acknowledgment. We are grateful (K.D.K., National Institutes of Health; A.D.Z., Swiss National Science Foundation) for research support. We are also thankful to Dr. Honorio V. Obias for initial observations.

Supporting Information Available: UV−vis spectra during the oxygenation of a 1:1 mixture of **1-(BArF)** and **2** (Figure S1), absorbance vs time in the stopped-flow kinetics experiment (Figure S2), and variable-temperature ^{1}H NMR information (spectra and δ vs 1/T plots) for **5-(CF_3SO_3)** and **6-(CF_3SO_3)$_2$** (Figures S3 and S4). This material is available free of charge via the Internet at http://pubs.acs.org.

IC981431+

(47) Evans, D. F. *J. Chem. Soc.* **1959**, 2003.

(48) *Handbook of Chemistry & Physics*, 74th ed.; Lide, D. R., Ed.; CRC Press: Boca Raton, FL, 1993.